A New Approach in Numerical Modeling of Inoculation of Primary Silicon in a Hypereutectic Al-Si Alloy

Faraji, M.

Original citation & hyperlink:
Faraji, M 2021, 'A New Approach in Numerical Modeling of Inoculation of Primary Silicon in a Hypereutectic Al-Si Alloy', *Metallurgical and Materials Transactions B*, vol. 52, no. 2, pp. 778-791.
10.1007/s11663-020-02052-y

DOI 10.1007/s11663-020-02052-y
ISSN 1073-5615
ESSN 1543-1916

Publisher: Springer

The final publication is available at Springer via http://dx.doi.org/10.1007/s11663-020-02052-y

Title: A new approach in numerical modelling of inoculation of primary silicon in a hypereutectic Al-Si alloy

Masoumeh Faraji

Dr Faraji is a lecturer in Mechanical Engineering and Materials at the School of Mechanical, Aerospace and Automotive Engineering,
and an associate member of Institute for Future Transport & Cities (FTC)

in Coventry University, Gulson Road, CV1 2JH, Coventry, United Kingdom

Corresponding email address: masoumeh.faraji@coventry.ac.uk

Abstract

The applicability of classical heterogeneous nucleation theory for an inoculated Al-18.6Si (wt%) alloy was investigated. Nucleation model proposed by Perepezko was used to study heterogenous nucleation of primary silicon in phosphorus-inoculated alloys. For this system, the nucleation temperature was found to be the most crucial variable in the model. If a spherical-cap model is assumed for heterogenous nucleation, then the contact angle changes only by the interfacial energy. However, the data applied to Perepezko's model showed it changed by undercooling. Therefore, it is suggested that the Perepezko's nucleation model is not applicable for analyzing data in inoculated hypereutectic Al-Si alloy.

Instead, for the first time, the free growth model developed by Greer to study the inoculation of Aluminum by Al-Ti-B was used for the Al-18.6Si (wt%) alloy inoculated with Al-Fe-P. The results of modelling compared with the experimental data showed that the free growth model gives a closer approximation when predicting the size of the primary silicon in the investigated alloy. Mechanical properties of as-cast hypereutectic alloys are influenced by size and shape of the primary silicon and eutectic silicon, type, size and frequency of entrainment defects and residual stresses. Finer silicon particles lead to higher tensile strength in the cast components. Being able to predict the size of primary silicon particles will facilitate control of the inoculation process, to enhance mechanical properties such as tensile strength. Developed model here provides a basis for predicting the size of primary silicon in hypereutectic Al-Si alloys treated with phosphorous-containing inoculants.

Introduction

Hypereutectic aluminum–silicon alloys are well known for their unique properties, namely, being light and having good wear resistance and thus, since 1970s, are widely used in the automotive industry pumps, compressors, transmission components, pistons and similar wear applications. Due to their microstructural arrangements, having hard primary silicon particles distributed throughout a eutectic matrix; some consider them in-situ metal matrix composites (MMC) where in addition to being light and having good wear resistance, they provide high elastic moduli, low thermal expansion and high resistance to elevated temperature service environments [1]. Fine primary silicon particles distributed evenly in these alloys improve their strength and machinability. Their hardness, tensile strength, yield strength and fatigue strength are comparable to other aluminum casting alloys.

Hypereutectic Al-Si alloys without any addition can have very large primary silicon particles, as large as even several millimeters. Unrefined silicon acts as stress-raiser impairing the mechanical properties. Refinement in hypereutectic Al-Si alloys (either by adding inoculants, such as phosphorus or increasing the cooling rate) reduces the size of primary silicon particles, which leads to an increase in the number of primary silicon particles and also morphological changes (from irregular plate-like or star-like to polyhedral) and consequently mechanical properties improvement [2]. For nucleation of primary silicon in hypereutectic Al-Si alloys, a level of undercooling is required. At a low level of undercooling, normally just a few particles are nucleated, so they will be large. Also, since the primary silicon is lighter than liquid aluminum, it travels upwards under buoyancy forces and causes segregation. Both results have negative effects on mechanical properties.

Different studies [3-5], found that phosphorus is one of the best refiners for these alloys. After addition, phosphorus forms AlP which precipitates in the melt and twinned silicon crystals are considered to nucleate on AlP. AlP is an effective heterogeneous nucleant for silicon because it has the same crystal structure (diamond cubic) and similar lattice parameter to silicon. The lattice parameter for silicon is 0.542 nm and for AlP it is 0.545 nm [5] and the melting point of AlP

(2530°C) is higher than the Al-Si hypereutectic liquidus temperature [6]. Ho and Cantor [7] revealed that they could trace phosphorus in the primary silicon particles using STEM X-ray elemental mapping and TEM. Nogita et al [8] reported the presence of P, Al and oxygen (O) in the eutectic silicon formed in a hypoeutectic Al-Si alloy, applying conventional energy-dispersive spectroscopy (EDS). Because AlP has a similar structure and lattice parameter to silicon, they assumed the nucleus was AlP and not $AlPO_4$. A more recent work by Wang et al [9] using STEM-EDX mapping analysis has shown that AlP nucleus, on which primary silicon particles were nucleated, contained nanoparticles with the near-stoichiometric Al_2O_3. Then, they speculated that the epitaxial growth of AlP particle is likely to occur on substrate of Al_2O_3 particles.

Xu et al [10] using in-situ micro-focus X-radiography studied the growth kinetics of primary Si particles during solidification of high-purity hypereutectic Al-Si alloys without and with P addition. They found the growth rate of inoculated samples to be lower which was attributed to two factors: the initial undercooling for primary Si particles growth was lower in the P inoculated alloy and inoculated alloy consumed more Si from the melt at low undercooling. Moreover, they argued that P inoculation increased the number density of primary Si particles and this resulted in easier solute impingement due to smaller spacing between neighboring particles.

Higher melt temperature (785°C and 850°C/1562°F) in Al-20 pct Si, to some extent, is found to have a positive effect on the size and distribution of the primary Si crystals particles which was attributed to presence of heterogeneous clusters of short range Si atoms existed above the liquidus temperature [11]. This was later shown using in-situ Neutron diffraction analysis of Al-

19 pct Si where solid Si was found present above the nonequilibrium liquidus temperature (672°C) due to the agglomeration of Si clusters in the melt [12-13].

Morphology of primary silicon is influenced by various factors including silicon content, undercooling, and cooling rate. It has been shown that low Si content would reduce branching in silicon morphology, this also requires low undercooling and low cooling rate [14].

In the present work the effect of phosphorus, as primary silicon refiner, on the microstructure and solidification behavior of Al-18.6 wt% Si alloy was monitored using cooling curves acquired during solidification and quantitative metallography. In addition, possibility of any systematic relation between number per unit volume (N_v) and the nucleation temperature (T_n) of primary silicon is investigated under different solidification conditions to predict the size of primary silicon particle.

Our earlier paper [15] reviewed the effect of cooling rate $\dot{T}$ and phosphorus inoculation on the number per unit volume $\overline{N_v}$ of primary silicon particles in hypereutectic Al-Si alloys. It was shown when combined with previously published data, the effect of cooling rate $\dot{T}$ and P addition on $\overline{N_v}$ is in reasonable accord with

$$\overline{N_v}/\dot{T} = (\pi/6f)^{1/2}10^{9}[250-215\ (\text{wt\%P})^{0.17}]^{-3} \quad \text{Eq. 1}$$

where f is volume fraction of primary silicon, $\overline{N_v}$ is in mm^{-3} and $\dot{T}$ is in K/s.

This work will be using two different nucleation models (i) classic nucleation model proposed by Turnbull [16] and developed by Perepezko [17] (referred here as Perepezko's model) and (ii) numerical model for inoculation in metallic system initiated by Maxwell and Hellawell [18] and developed by Greer [19] (referred here as Greer's model), free growth model for inoculation of aluminum by optimized Al-Ti-B grain refiners, to predict the size of primary silicon in inoculated hypereutectic Al-Si alloys.

Experimental and Results

This section is divided into three sub-sections which will describe the procedures of sample preparations and the testing and data collection procedures. This will be followed by detailed description of the nucleation models that were utilized in this work, enlisting equations and data applied to develop a model(s) specifically for P inoculation in hypereutectic Al-Si alloys to predict size of primary silicon particles after solidification.

I. Material Preparation

Al-18.6Si-0.02Cu-0.0014P (wt %) supplied by Norton Aluminum Products was used as the melt, with Al-6.75Fe-4.91P (wt %) supplied by KB Alloys as primary silicon refiner. AlFeP was chosen as the P inoculant based on the experimental results published by Kyffin et al [20] showing that AlFeP provided higher level of refinement than AlCuP inoculants, particularly for an alloy with similar chemical composition to the studied alloy. The Al-Si alloy (150g) was melted in a stoppered alumina crucible positioned in a resistance heated vertical tube furnace. The melt temperature was 800°C. After allowing 15 min contact time for each addition the treated melt was cast into a Quik-Cup sand mold placed below the melting crucible by withdrawing the stopper rod. The dimensions of the mold cavity were 40mm×35mm with a built-in silica sheathed thermocouple on the central axis of the mold. Figure 1 shows schematically the bottom casting apparatus used [15] and Figure 2 shows the procedure of casting using this apparatus. An alternative casting method was also used to reduce the effect of turbulence during casting in which a stainless steel cup (bore: 30mm, height: 30mm) with a cold charge of metal (30 g) with a ceramic-fiber lid (thickness: 13mm) was put into a chamber furnace set to 800°C. Inoculation of the melt was done outside the furnace by plunging 0.02-0.08 wt% P wrapped with aluminum foil into the melt. The aluminum foil was used to ensure that the small pieces of inoculant could all be plunged into the melt. This may have an impact on the number of heterogeneities introduced to the melt. But given that the same inoculation procedure was used for all samples, the role of inoculation can be studied with good accuracy as they were mostly compared with each other. Moreover, a very clean and small foil was used to ensure that the contamination was minimized, and the data could be used elsewhere. After 15 min in the furnace the mold was removed and placed onto a copper block (thickness: 35mm, diameter: 75mm) to solidify. Metallographic characterization of the ingots was done by longitudinal sectioning, grinding, and polishing. Measurements of the numbers of particles per unit area (N_A) were made with an Olympus VANTOX-T microscope connected to an Iiyama computer with an image grabber and KsRun 3 image analysis software. For each value of N_A, 15 micrographs were point counted by hand to give an average N_A. For each sample, numbers of primary silicon particles per unit volume (N_V) were determined from N_A using $\overline{N_V} = \left(\frac{\pi}{6f}\right)^{1/2} \overline{N_A}^{3/2}$ Eq. 2 [21] where f is the volume fraction of primary silicon phase.

Figure 3 presents optical micrographs for microstructures of six different samples cast under different casting conditions and with different level of inoculations: no addition, 200, 400 and 800 ppm P inoculated by AlFeP, cast in sand mold and steel mold. Their detailed casting information and metallographic measurements are provided in Table 1. This Figure clearly shows that the highest level of refinement in this alloy was achieved by 800 ppm inoculation.

Figure 4 shows the cooling curve for one of the samples inoculated with 800 ppm P (sample named as S10: details in Table 1). Formation temperature of primary silicon phase (T_n) was determined for each sample from the first and second derivatives of cooling curves. Figure 5 shows part of the cooling curve with its first and second derivatives which plotted using MATLAB for one of the samples (S10) to identify T_n. The liquidus temperature (T_L) of the alloy was calculated as the assessed equilibrium value [22] given by the following equation [23]:

$$T_L = T_{EU} + 14.93(C-C_{EU})-9.28\times10^{-2} (C-C_{EU})^2+3.59\times10^{-4}(C-C_{EU})^3 \qquad \text{Eq. 3}$$

where T_L: liquidus temperature (°C); T_{EU}: equilibrium eutectic temperature, 577.1°C; C; alloy composition (at%) and C_{Eu}: equilibrium eutectic composition, 12.2 at.% Si. For this alloy (18.6 wt%≡18 at%: the average value for silicon composition), Eq. 3 gives T_L as 660.7°C. Then, the undercooling for primary silicon formation (ΔT_n) was obtained as T_L-T_n for each sample.
In addition, the cooling curves were used to determine the cooling rate of cast ingots using its slope ($\dot{T}$) from the peak temperature (T_P) to T_n. Figure 6 provides a schematic cooling curve showing temperatures, T_P, T_L, T_n and T_{Eu}.

The conditions studied, cooling curve and quantitative metallographic results are listed in Table 1.

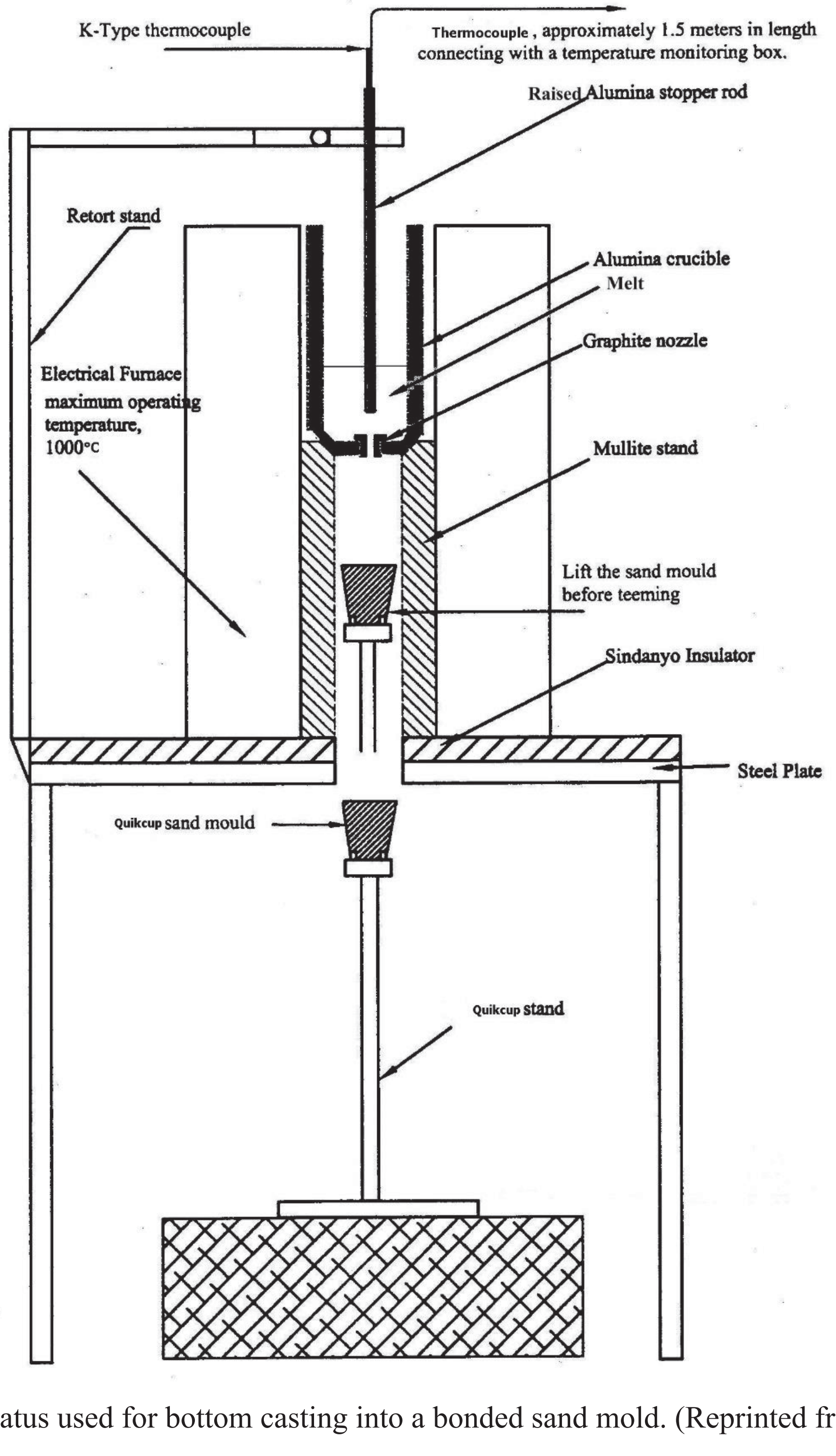

Fig. 1 Apparatus used for bottom casting into a bonded sand mold. (Reprinted from [15]).

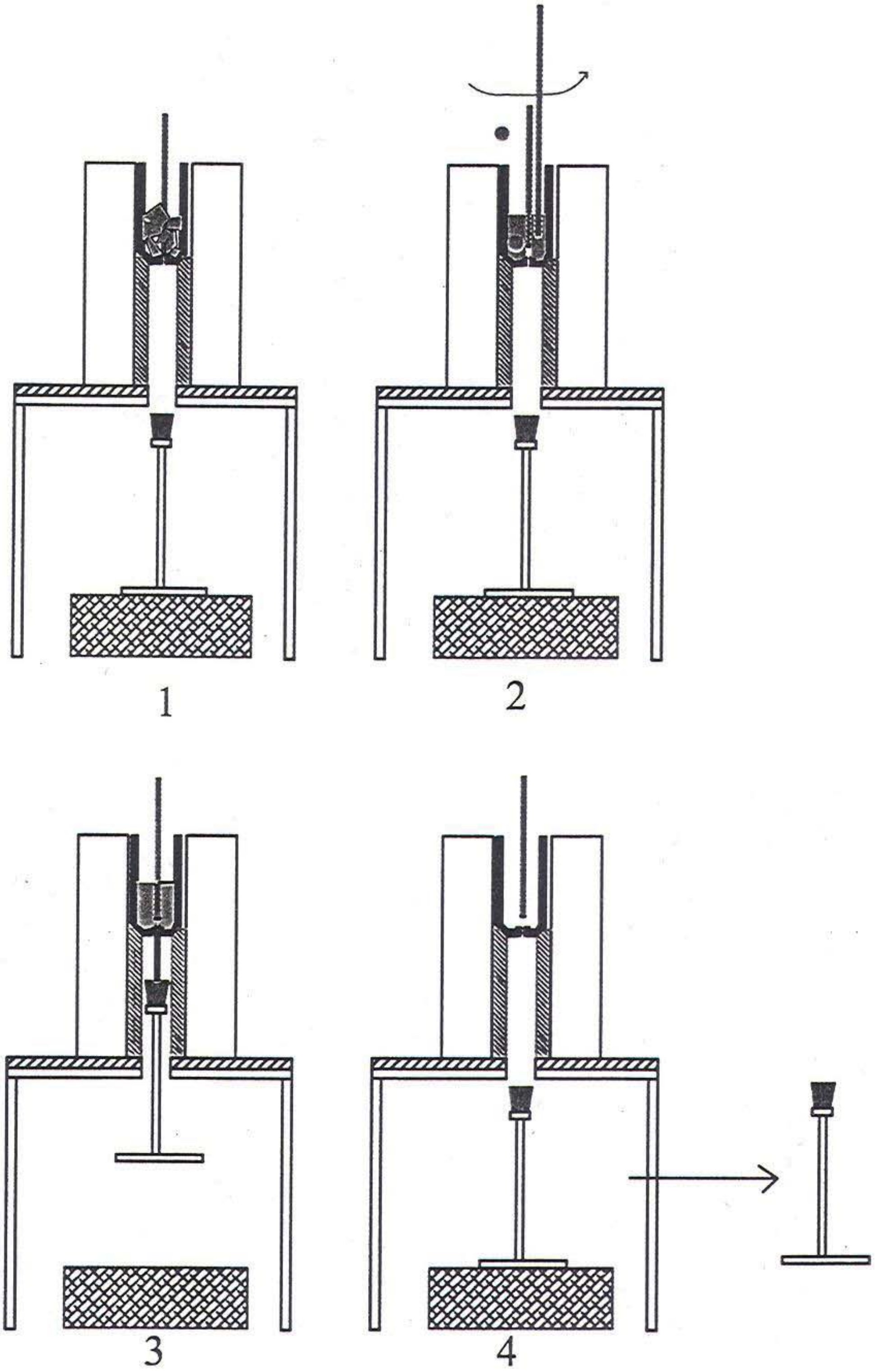

Fig. 2 Casting procedure used for bottom casting in this work. (1- re-melting of the hypereutectic Al-Si alloy, 2- Adding Phosphorus inoculant in Al foil, 3- removing the stopper rod, 4- removing the sand mold.)

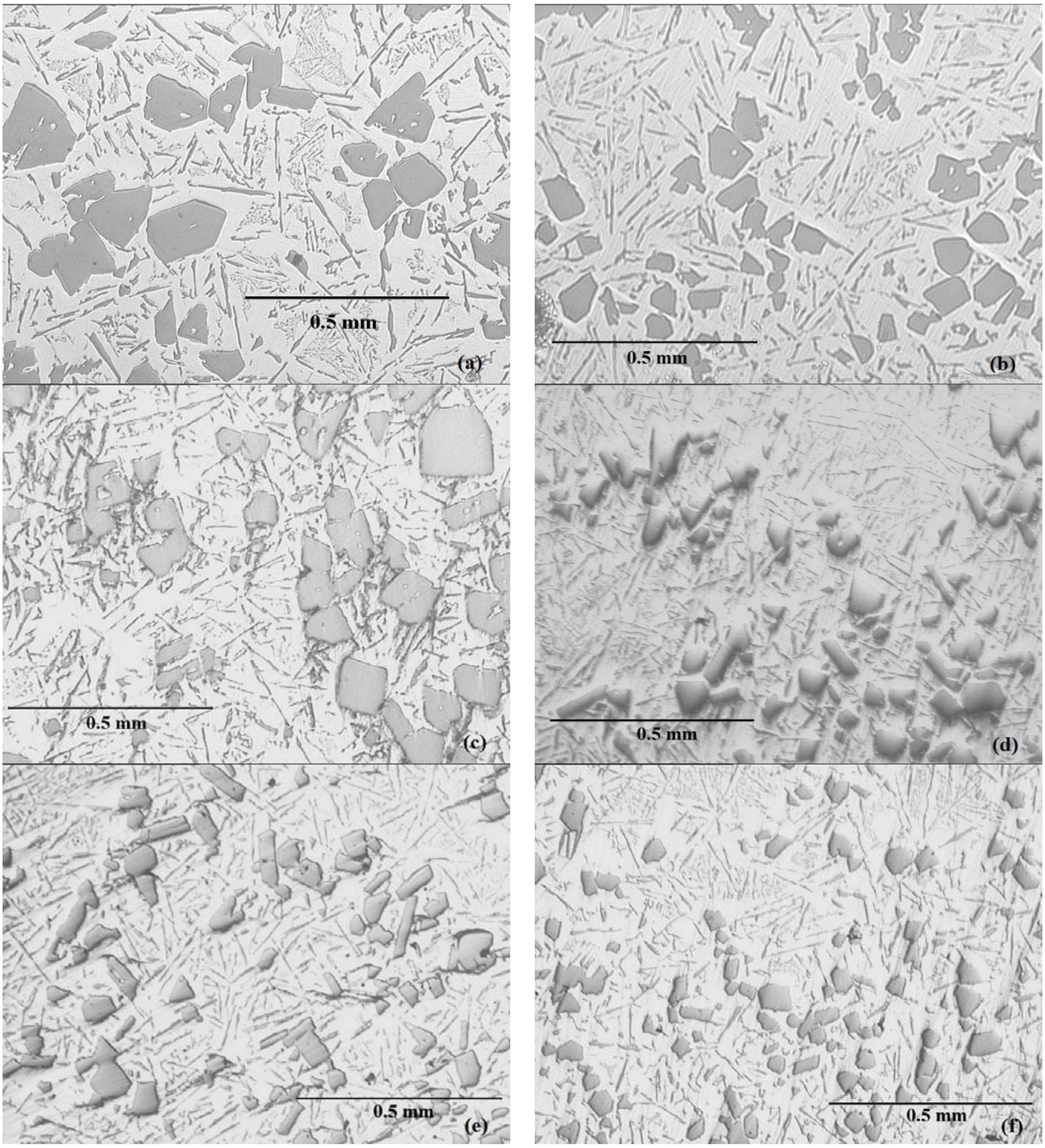

Fig 3. showing different microstructure from samples cast using two different molds (sand and steel molds) and three different inoculation levels: a- taken from sample C3 cast in sand mold with no inoculation, b- taken from sample C6 cast in sand mold with 200 ppm inoculation with AlFeP, c to f taken from samples (S3, S5, S9 and S10, respectively) cast in steel molds in the furnace with no addition, 200 ppm, 400 ppm and 800 ppm, respectively. The figure clearly shows that the highest level of refinement was achieved by addition of 800 ppm P (sample S10 shown in f). Table 1 has provided all the casting conditions, as well as number density for these samples.

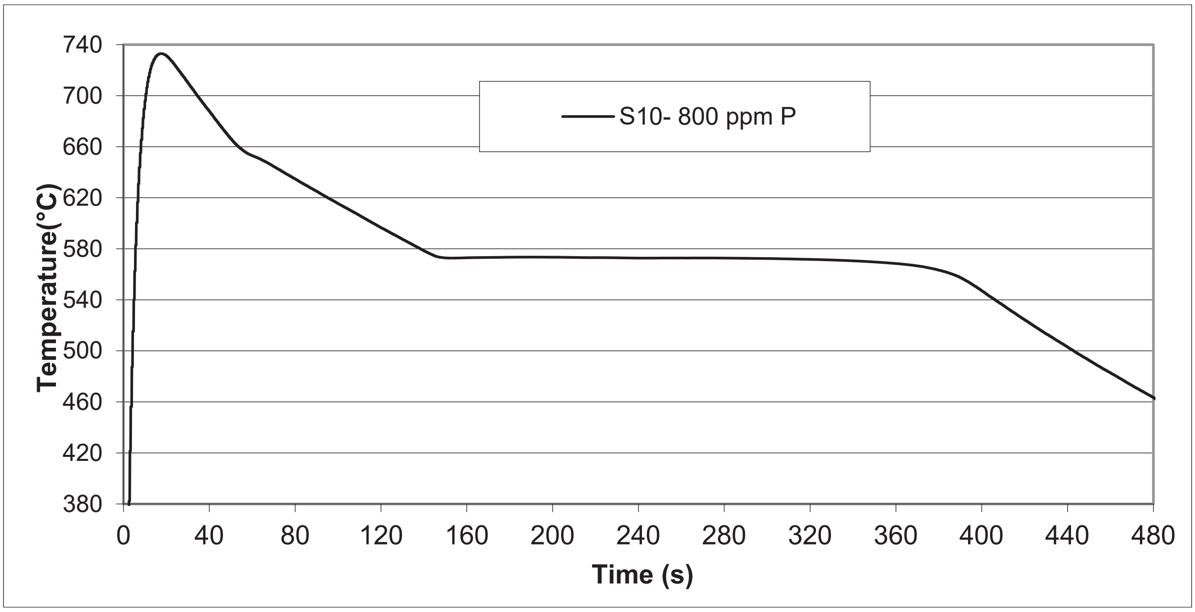

Fig. 4 the cooling curve for one of the samples inoculated with 800 ppm P (sample named as S10: details in Table 1).

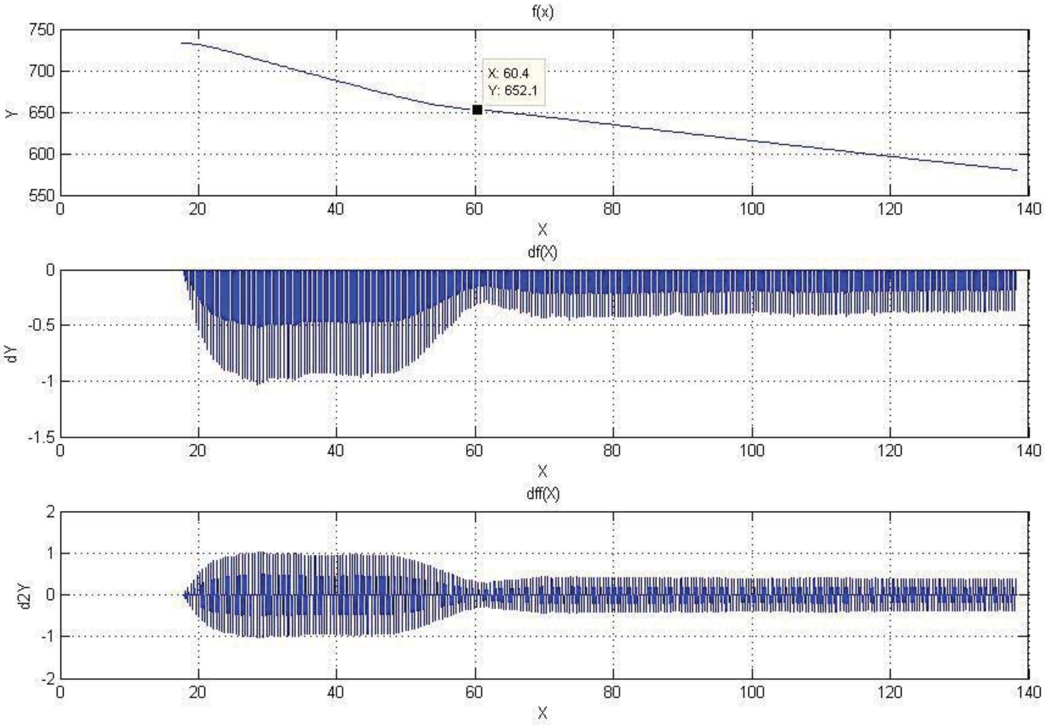

Fig. 5 part of the cooling curve (from the peak temperature to temperatures above eutectic) with its first and second derivatives for one of the samples (S10) to identify T_n, plotted using MATLAB.

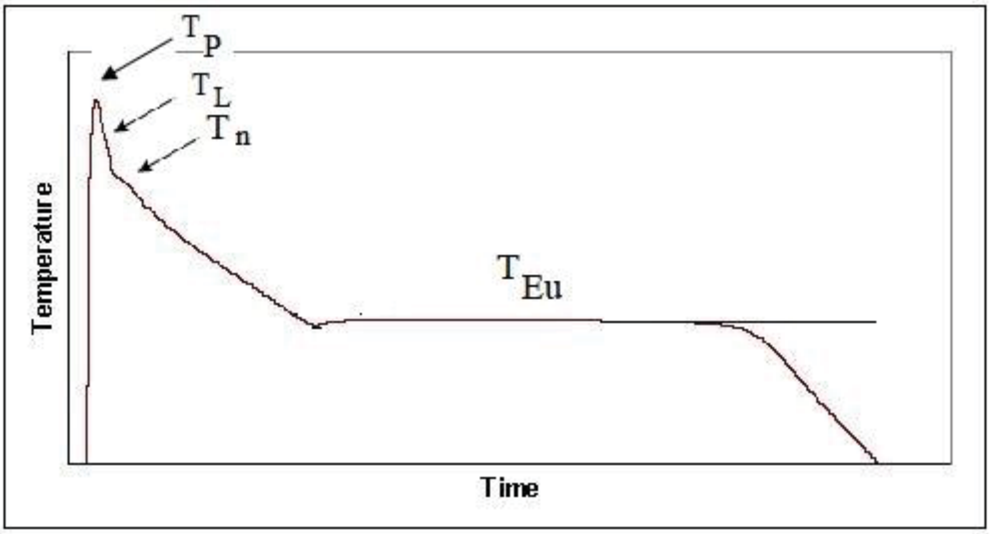

Fig. 6 Schematic cooling curve showing temperatures T_P, T_L, T_n and T_{Eu}.

II. Nucleation Kinetics

The heterogeneous nucleus is usually modelled as a spherical cap on a flat substrate with a wetting (or contact) angle θ (Figure 7 adapted from [24]).

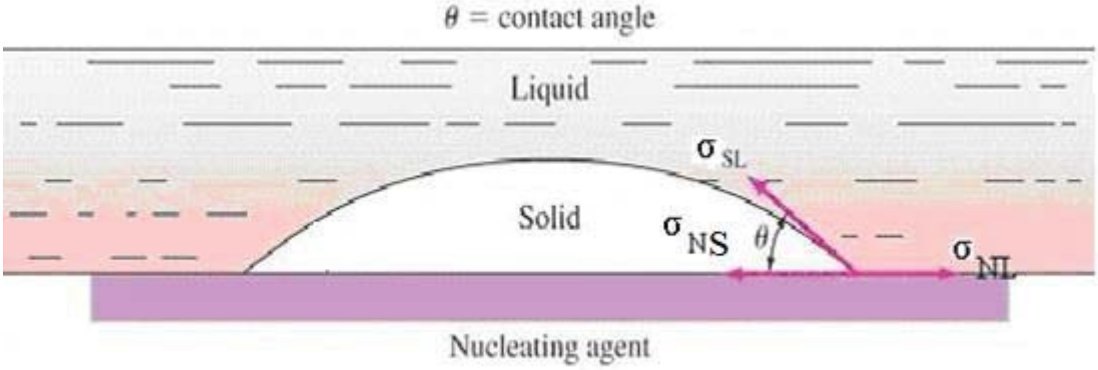

Fig. 7 Heterogeneous nucleation of a spherical cap on a nucleating agent (adapted from Fig. 2, Ref. 24).

Then:

$$\sigma_{NL} = \sigma_{SL}.\cos\theta + \sigma_{SN} \qquad \text{Eq. 4}$$

where σ_{NL}, σ_{SN} and σ_{SL} are the nucleant-liquid, solid-nucleant and solid-liquid interfacial energies per unit area respectively and θ is the contact angle. The formation of the above-mentioned spherical nucleus has an excess free energy as follows:

$$\Delta G_{het} = \{-4\pi/3\, r^3 \Delta G_V + 4\pi r^2\, \sigma_{SL}\}\ f(\theta) \qquad \text{Eq. 5}$$

where $f(\theta) = [2 - 3\cos\theta + (\cos\theta)^3]/4$ Eq. 6

and ΔG_V is the free energy change on solidification per unit volume. The principal purpose of a nucleant is to increase the nucleation frequency (I) [25]. The nucleation behavior of alloys in steady state has been modelled by many researchers including Perepezko [17] which I is defined [26] by:

$$I = \Omega\, exp\left(\frac{-\Delta G*}{kT}\right)$$ Eq. 7

where ΔG* is the nucleation barrier which is given as follows:

$$\Delta G^* = \frac{16\pi\sigma_{SL}^3}{3\Delta G_V^2} f(\theta)$$ Eq. 8

σ_{SL} is the solid-liquid interfacial energy per unit area, and k is Boltzmann's constant (1.3806×10^{-23} J/atom K) . For surface-dependent heterogeneous nucleation, the prefactor is expressed [17, 27] as:

$$\Omega_a = \rho\left(\frac{D_L}{a^2}\right)\left(\frac{8\pi\sigma_{SL}^2(1 - cos(\theta))}{\Delta G_V^2 . a^2}\right)$$ Eq. 9

where ρ is the heterogeneous site density, D_L is diffusivity of solute in the melt which can be gained from an Arrhenius relationship, a is jump frequency and θ is the contact angle. Using calculations for nucleation of Bi-40 at% Cd, Perepezko and Tong [27] determined ρ as 5.7×10^{19} m^{-2} which considered as 10^{20} in [17], [23] and our results.

Equations 7 and 9 show that the heterogenous nucleation frequency depends on the liquid properties, solid-liquid interfacial energy, free energy change on solidification, total number of atoms in contact with unit area of nucleant surface (ρ) and the contact angle.

Then, for volume-dependent heterogeneous nucleation (e.g. in rapid solidification processing, spray deposition and surface melting), the prefactor is expressed [16, 28] as:

$$\Omega_V = \left[\frac{2D_L}{V_L}\left(\frac{\sigma_{SL}}{kT}\right)^{1/2}[f(\theta)]^{1/6}\right][A_P N_v^{'}]Z(1 - f_s)$$ Eq. 10

where V_L is the atomic volume of an atom in the liquid, A_p is the surface area per mole, f_s is solid fraction, and Z is the Zeldovich factor (which corrects the equilibrium nucleation rate for nuclei that grow beyond the critical size). Z is calculated [29] via:

$$Z = \sqrt{\frac{-1}{2\pi kT}\left(\frac{\partial^2\Delta G}{\partial n^2}\right)_{n*}}$$ Eq.11

where n is the number of atoms in an embryo, n* is the number of atoms in the nucleus. $N_v^{'}$ in Eq. 10 is the number of catalytic motes per unit volume which is given [30] by:

$$N_v^{'} = N_V^0\, exp(\beta\Delta T)$$ Eq. 12

where N_V^0 is a base level of nucleants estimated to be to 10^{13} m^{-3}, β is a positive constant and ΔT is the melt undercooling [31].

As it can be seen comparing equations 9 and 10, the prefactor in equation 10 is temperature dependent, this prefactor is used for processes such as rapid solidification or in the nucleation of metallic glass [32]. Therefore, given that solidification in this work was not rapid equation 9 (prefactor for surface-dependent nucleation) was used to predict the heterogeneous nucleation frequency given in equation 7.

Assuming a constant cooling rate $\dot{T}$, the number of nuclei per unit area/volume (depending on I) N [33] is expressed as:

$$N = \frac{1}{\dot{T}} \int_{T_n}^{T_L} I \, dT \qquad \text{Eq. 13}$$

To study the effect of solidification parameters on the number of primary silicon particles, Liang et al [23] applied the heterogeneous surface-dependent model (embodied in Eq. 9) to their results for nucleation of primary silicon in Bridgman solidified Al-18.3 wt% Si. Based on these results, they concluded that increasing undercooling from 35 to 52 K over the range $1 < \dot{T} < 20K/s$, was associated with an increasing θ from 26 to 36°. In their work, they did not independently determine θ, values for θ were estimated through determining values for N from the microstructures and then fitting the data into surface-dependent nucleation equations 7-9 and 13.

Gremaud et al [28] conducted a study on nucleation and growth kinetics of a laser-produced uninoculated Al-26 wt% Si alloy which was rapidly solidified. They applied the heterogeneous volume-dependent approach for the nucleation process (Eq. 10). Their analysis predicted 71.3° for the value of θ on the spherical cap model with 215 K undercooling at a temperature gradient of 2×10^{6} K/m.

In another example, Ho and Cantor [34] recorded a value of 43° for θ and a nucleation density of 2×10^{-11} per droplet for nucleation of silicon in Al-3wt%Si alloy with an undercooling of 60 K, at cooling rate over the range 4-15 K/min using classical heterogeneous nucleation theory (Eq. 9) developed by Perepezko [17].

It is worth to note that modelling heterogenous nucleation using classical theory is based on stochastic addition of molecules to initially sub-critical embryos. It assumes nucleant as a spherical cap where its efficiency, for a given cooling rate, depends on its potential as a substrate- expressed by the angle of contact between the nucleated particles and substrate- and the environment in which the nucleation occurs; i.e. the alloy constitution [18]. As shown in equations 7 and 8 the nucleation frequency is very sensitive to the interfacial energy as solid-liquid interfacial energy is cubed (in Eq. 8) which will go into the argument of the exponential (in Eq. 7). This makes using this model difficult as direct determination of σ_{SL} is not easily manageable. Moreover, this work will be showing that theta is not the only main factor influencing the nucleation frequency in inoculated Al-Si alloys.

III. Primary silicon size prediction

To predict the size of inoculated primary silicon particles after solidification, two main models, Perepezko's surface-dependent model and Greer's free growth model, are applied in this work. To validate the results of the models, at the end of solidification the number density of primary silicon per unit area and the volume fraction of primary silicon phase have been measured using microstructural analysis of the samples. N_V is calculated using Eq. 2 and then using the following equation the size of primary silicon particles has been calculated:

$$N_V = \frac{4}{\pi}\left(\frac{2}{3}\right)^{1/2}\left(\frac{f}{D_A^3}\right) \quad \text{Eq. 14 [35]}$$

where D_A is the mean diameter of silicon particles. The results of the measured values for the size of particles and their number density were used to compare them with the predicted data obtained from both Perepezko's and Greer's models.

A. Modelling based on Perepezko's model

Perepezko's model theoretically is developed model heterogenous nucleation; this model could predict the nucleation frequency and the particle density of heterogenous nucleation as shown in Equations 6 to 14 if properties of the melt and the nucleant are known. In this work, calculated values for number per unit area of primary silicon particles was applied to this model through Equations 6 to 9 and 13-14, to determine the efficiency of the nucleants through estimation of θ. According to Perepezko's model with a very low undercooling a smaller contact angle is expected to be consistent with heterogeneous nucleation. To visualize the effect of the formation temperature of primary silicon (T_n) or undercooling in this model Figure 8 plots the calculated contact angles versus undercooling of primary silicon for the present work and that of other workers. Theta is the contact angle calculated by surface-dependent nucleation model and the conditions were; Liang et al [23]: Al-18.3 wt% Si, no P addition, $\dot{T}$: 0.6-18.9 K/s, Kaneko et al [36]: Al-19 wt% Si, 0.02 wt% P addition, $\dot{T}$: 0.017-1.67 K/s, Ohmi et al [37-39]: Al- 32 wt% Si, Al- 22 wt% Si, uninoculated, $\dot{T}$: 10.7-198 and 13.1-221 K/s, respectively.

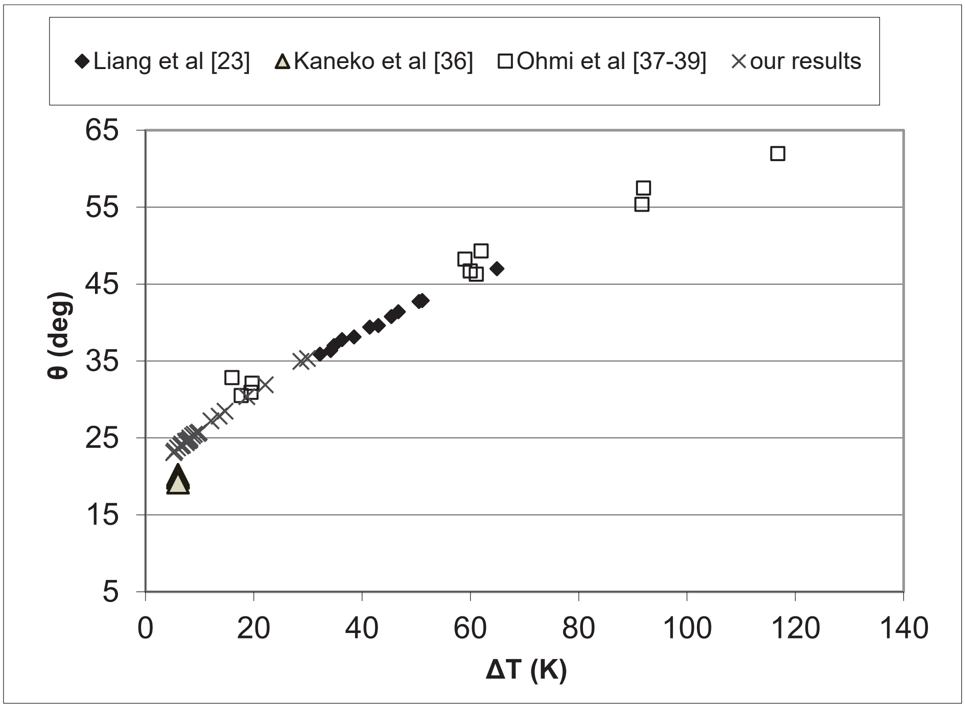

Figure 8 The change of contact angle with undercooling for the formation of primary silicon for our results and those of other workers, (the contact angle calculated from the surface-dependent nucleation model.). Liang et al [23]: Al-18.3 wt% Si, no P addition, $\dot{T}$: 0.6-18.9 K/s, Kaneko et al [36]: Al-19 wt% Si, 0.02 wt% P addition, $\dot{T}$: 0.017-1.67 K/s, Ohmi et al [37-39]: Al-32 wt% Si, Al-22 wt% Si, uninoculated, $\dot{T}$: 10.7-198 and 13.1-221 K/s, respectively.

Using Eqns. 6-13, with the following simplifications after Gremaud et al [28], the contact angle was calculated:

Although the integral in Eq. 13 may be evaluated numerically, it can be approximated by:

$$\int_{T_n}^{T_L} I\,(T).dT \cong (T^{'} - T_n)I_V(T_n) \qquad \text{Eq. 15}$$

where T′ is the intersection between the tangent of I(T) at T_n and the temperature axis. This approximation implicitly neglects the contribution of nuclei between T_L and T′. Assuming that σ_{SL} and Ω are independent of temperature over the temperature range of interest, differentiation of Eq. 15 gives:

$$I(T_n)V.t = -\frac{b.(\sigma_{SL}^3).f(\theta).\Delta T\left[2T_n\frac{d\Delta G_V}{dT}+\Delta G_V\right]}{k(\Delta G_V^3)T_n^2} \qquad \text{Eq. 16}$$

It should be added that Liang et al [23] used a general equation for binary metallic alloys, introduced by Thompson and Spaepen [40], to calculate Gibbs free energy (ΔG_V) per unit volume for formation of primary silicon from liquid Al-Si in which they assumed a constant entropy of fusion (ΔS_V) of the melt, although ΔS_V varies with temperature [41], whereas, Murray and McAlister [22] introduced thermodynamic parameters to calculate ΔG_V for binary Al-Si alloys. Therefore, in this work the thermodynamic parameters of Al-Si alloy given in Murray and McAlister [22] (Table 2), and used by Gremaud et al [28], were used to calculate ΔG_V. The required data for calculations is given in Table 3.

Due to the process condition for this work and those other works used to plot Figure 8, it was concluded that the nucleation of silicon is a surface-dependent heterogeneous nucleation. Then using Eqs 6 through 13 Nv for the primary silicon particle could be calculated if the value for the theta (contact) angle was known. Therefore, it was decided to use an estimated theta for each condition. After plotting a graph of contact angle versus undercooling using the data gathered from Liang et al [23], Kaneko et al [36], Ohmi et al [37-39] and some part of the current study (shown in Figure 8), an estimate can be obtained by 4th degree polynomial fit for the drawn curve (Figure 9):

$$Theta = a \times \Delta T^4 + b \times \Delta T^3 + c \times \Delta T^2 + d \times \Delta T + e \qquad \text{Eq. 17}$$

where a, b, c, d and e are -6.40E-07, 0.0001616, -0.01482, 0.924483 and 17.44898 respectively.

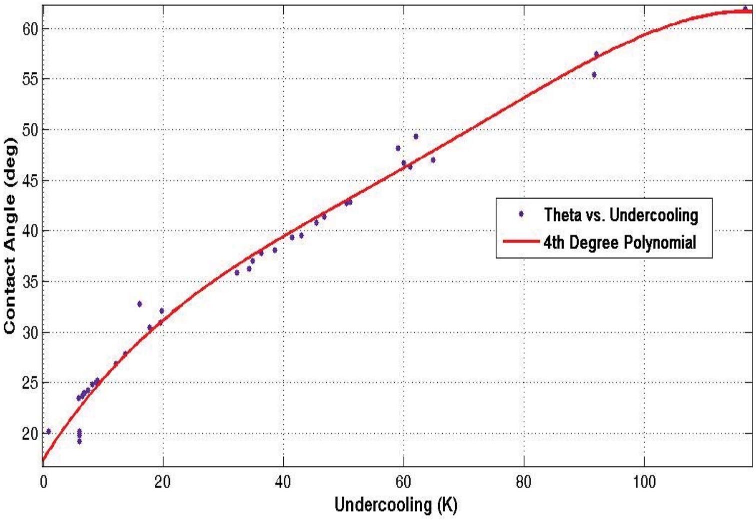

Figure 9: A line fitting to identify the trend of the curve correlating the change of contact angle with undercooling for the nucleation of primary silicon for our results for specimens of C1 through C8, and D3 through D5 and those of other workers, details are given in Figure 8.

Then using calculated Nv the diameter/radius for the primary silicon particles can be obtained by Eq. 14. Table 4 summarizes the predicted data, using Perepezko's model, for the particle radius and compares it with the values measured experimentally. Figure 10 depicts these data versus the undercooling. As it can be seen in Figure 10, there is a considerable difference between values measured and predicted; especially for undercooling higher than 15K. Also, for undercooling below 15K predicted values are much smaller than the measured counterparts. Therefore, it was decided to undertake a different approach and use a different model that has been used for aluminum alloys but for different chemical composition, and different types of inoculants.

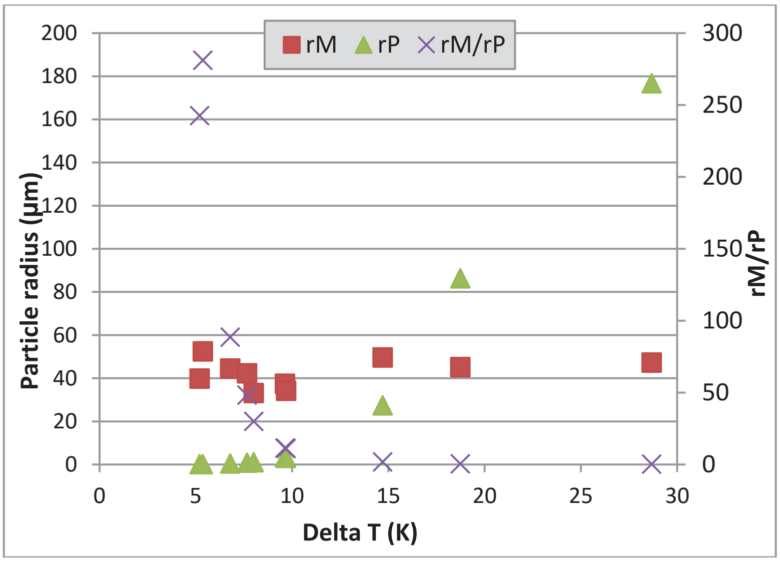

Figure 10: Measured and predicted particle size versus undercooling for conditions shown in Table 1 and results from Table 4. Predictions are made using Perepezko's nucleation model. r_M and r_P represent measured radius and predicted radius, respectively. It shows a significant difference between predicted and measured values for particle radius for undercooling higher than 15K.

B. Modelling based on Greer's model

The modelling in this section is based on the equations developed by Greer et al [19, 42] to predict the grain size of inoculated aluminum alloys. They placed the model on the factors influencing the grain size in the melt: i.e. the cooling rate of the melt, its solute level, and the amount of added inoculant. This model is shown to work well for effective inoculants in which the initial crystal nucleation was limited by the free growth of the crystal and not by nucleation itself; hence, nucleation was not stochastic. In this model the critical undercooling for the nucleation can be determined by the particle (inoculant) size which is measurable; whereas in the Perepezko's model the critical undercooling is dependent on the contact angle which is difficult to measure or predict with reasonable accuracy. Conversely, Greer's model requires size distribution knowledge of the inoculants.

Greer's model assumed that at any time the melt could be taken as spatially isothermal in which latent heat release and external heat extraction were considered during the thermal modelling. They have shown that the model is able to predict the grain size of inoculated small-volume melts.

Upon cooling the melt below the liquidus temperature, free growth of crystal begins initially on the largest inoculant particles, followed by on more, smaller particles. This growth results in latent heat being released, which slows the cooling rate, and ultimately increases the temperature (recalescence occurs). At this stage there is no further free growth initiation and hence grain refinement becomes limited. This model, therefore, uses calculations of the crystal growth rate to numerically predict the grain size [19].

Following paragraphs provide equations and parameters required to undertake this modelling which then is adapted to nucleation of primary silicon particles nucleated on AlP nucleants.

Growth rate equations are taken from [19]. Similar to Greer's, for this work it has been assumed that the silicon grows in a spherical manner with the radius of r, then the growth rate (*V*) is calculated as follows:

$$V = \frac{\lambda_S^2 . D_S}{2r} \qquad \text{(Eq. 18)}$$

where D_s is the solute diffusion coefficient in the liquid, and λ_s is a parameter obtained using the invariant-size approximation as follows:

$$\lambda_s = \left(\frac{-S}{2\pi^{1/2}}\right) + \left(\frac{S^2}{4\pi} - S\right)^{1/2} \qquad \text{(Eq. 19), where S is given by}$$

$$S = \frac{2\left[\frac{\Delta T - \Delta T_C}{m}\right]}{(k-1)\left(\frac{\Delta T - \Delta T_C}{m} + C_\circ\right)} \qquad \text{(Eq. 20)}$$

where C_0 is the solute content in the alloy melt, m is the liquidus slope, k is the equilibrium partition coefficient and ΔT is the overall melt undercooling and ΔT_c is the curvature undercooling [19] and is given by

$$\Delta T_c = \frac{2\sigma}{\Delta S_v . r} \qquad \text{(Eq. 21)}$$

where ΔS_V is the entropy of fusion per unit volume. Similar to Greet et al [19], the calculations here are performed for a notional melt volume of $1 m^3$ and the melt is treated as a series of short isothermal steps with duration of dt.

$$T_{n+1} = T_n - Rdt \qquad \text{(Eq. 22),}$$

$$r_{n+1} = r_n - Vdt \qquad \text{(Eq. 23)}$$

r is the radius of the particle, which is growing, R is the cooling rate and σ is solid-liquid interfacial energy, here is considered as 0.3524 J/m^2 [43].

These calculations consider that for each set or particles, crystal growth begins on them as soon as the melt undercooling reaches or exceeds their free growth undercooling (ΔT_{fg}) which can be calculated as follow [19]:

$$\Delta T_{fg} = \frac{4\sigma}{\Delta S_V . d} \qquad \text{(Eq. 24)}$$

where d is the diameter of the particle.

For these calculations, the formation temperature of primary silicon is considered as T_n, and the size of AlP particle for each amount of addition is the first r_n, and dt is 0.1 s. The remaining assumptions are C_0 as 0.816 (for Al), m for Al-Si in the other part of the graph- hypo- is taken from Al-Si phase diagram as liquidus slope for Al (measured as -13.2), and k (solute partition coefficient) = 4×10^{-5} [44] k is adapted from k for Al in S-Al alloys as 4×10^{-5} at the Si liquidus of Al-26 wt% Si from diagrams produced by Murray and McAllister [22].

It should be noted that where the diameter of the nulceant (AlP) was needed, Kyffin et al's [45] paper was used. Kyffin et al [45] measured diameter of AlP particles which were between 6 to 9 micron with adding 200 ppm and 500 ppm P as Al-Fe-P and between 9 to 12 with adding 800 ppm P; therefore, in this work the calculations for 200 and 400 ppm inoculated specimens (200ppm: S4, S6, S6, S13, S14 and S15, 400ppm: S7, S8 and S9) are based on the nucleant diameter of 7.5 micron and for 800 ppm inoculated samples (S10, S11, and S12) 10.5 micron. Although there is no measurement for untreated specimens in their case here $2r$ is assumed to be

4.5 micron for unrefined specimens (S1, S2 and S3: where they already had 15 ppm P). It should be noted that, similar to Kyffin et al [45], Al-Fe-P was used as silicon inoculants for this work.

Entropy of Fusion (*ΔS_v*) Calculations for Si and Al in Solid and Liquid State

Considering T is given in K, and using the C_P given in Table 5 [46], entropy of fusion for each element in solid and liquid state is calculated as:

$$S_{Al}^{S} = 28.34 + 20.67Ln\left(\frac{T}{298}\right) + 12.39 \times 10^{-3}(T - 298) \quad \textbf{(Eq. 25)}$$

$$S_{Al}^{L} = 165.06 + 31.8Ln\left(\frac{T}{298}\right) \qquad \textbf{(Eq. 26)}$$

$$S_T = S_{298} + \int_{298}^{T} C_P d\, ln\, T \qquad \textbf{(Eq. 27)}$$

If $C_P = a + bT + cT^{-2}$ J/mol K **(Eq. 28)**; therefore entropy is calculated as:

$$S_T = S_{298} + aLn\left(\frac{T}{298}\right) + b(T - 298) - \frac{1}{2}c\left(\frac{1}{T^2} - \frac{1}{298^2}\right) \qquad \textbf{(Eq. 29)}$$

$$S_{Si}^{S} = 18.84 + 23.94Ln\left(\frac{T}{298}\right) + 2.47 \times 10^{-3}(T - 298) - \frac{1}{2}(-4.14 \times 10^5)\left(\frac{1}{T^2} - \frac{1}{298^2}\right) \ \textbf{(Eq. 30)}$$

$$S_{Si}^{L} = 168.5 + 25.62Ln\left(\frac{T}{298}\right) \qquad \textbf{(Eq. 31)}$$

In the end, to use **ΔS_v** at Eq. 21, the following Equation is used:

$$\Delta S_V = \left(C_{Al} * (S_{Al}^{S} - S_{Al}^{L})\right) + \left(C_{Si} * \left(S_{Si}^{S} - S_{Si}^{L}\right)\right) \qquad \textbf{(Eq. 32)}$$

C_{Al} was 0.814 and C_{Si} was 0.186, therefore; to be able to use Eq. 32 in Eq. 21 it should be converted from J/mol K to J/m^3, this is done by multiplying the outcome of Eq. 32 by 82896.9.

ΔT in Eq. 20 is calculated using the following equation:

$$\Delta T = T_L - T_n \qquad \textbf{(Eq. 33)}$$

where T_L is the liquidus temperature and T_n is the actual temperature during the solidification.

Diffusion coefficient of Si in Al-Si alloys (D_s)

Interdiffusion coefficients in Al-Si alloys were determined by Fujikawa et al [47] using Matano's method in the temperature range of 753 to 893 K. They have calculated the following equation by extrapolating the concentration dependence of the impurity diffusion coefficient to zero mole fraction of Si:

$D_{Si/Al} = (2.02^{+0.97}_{-0.66}) \times 10^{-4} exp\lfloor -(136 \pm 3) kJ\ mol^{-1}/RT \rfloor m^2/s$ **(Eq. 34)**

In Eq. 34 there is a limit at which the boundaries are set. Hence, the boundaries for the current study were set via trial and error, resulting in the following equation:

$D_{Si/Al} = (2.55) \times 10^{-4} exp\lfloor -(136) kJ\ mol^{-1}/RT \rfloor m^2/s$ **(Eq. 35)**

The temperature range used in the present study was ~840-930 K. Nevertheless, the Eq. 35 was found a reasonable method of calculating the diffusion coefficient of Si in Al-Si alloys.

For this study, and for Greer's model the growth of primary silicon considered to begin from the nucleation point of the primary silicon and end at the eutectic arrest. Table 6 summarizes the numerical data obtained from this modelling and Figure 11 depicts these data. The results show that there is a good correlation between the predicted particle size with those measured. It is worth to note that compared to Perepezko's model, Greer's model delivers closer results to size of measured primary silicon particles.

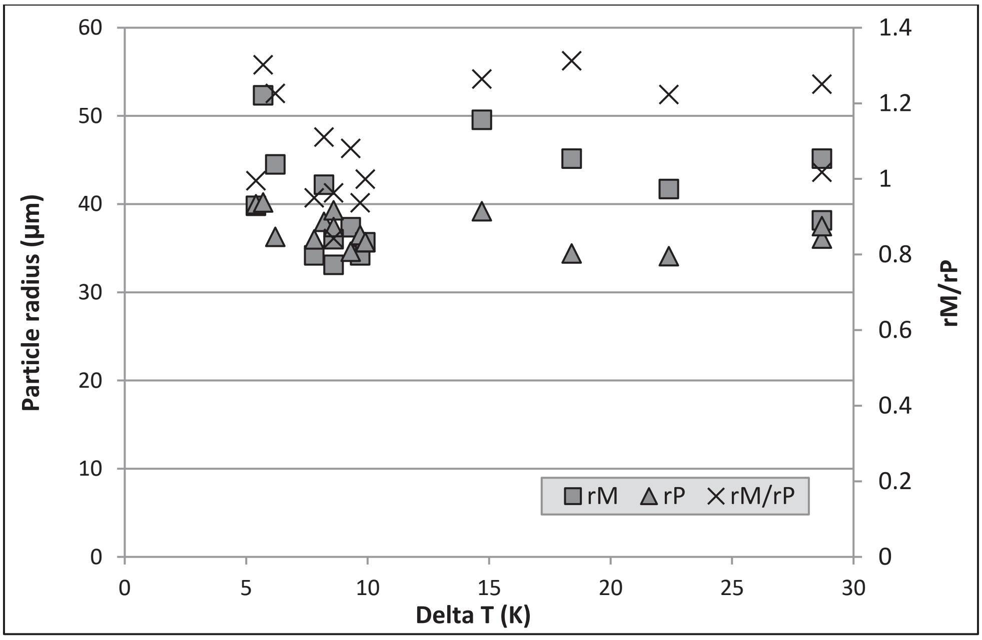

Figure 11: Measured and predicted particle size versus undercooling for conditions shown in Table 6, Predictions are made using Greer's nucleation model: r_M and r_P represent measured radius and predicted radius, respectively.

Discussion

Heterogenous nucleation usually is investigated through considering a spherical cap model nucleation on the surface of a planar nucleant. A previous work [48] has shown that the spherical

cap model is not applicable for potent nucleation, i.e. very small theta angle, as for θ≤10° the nucleus reduces to a monolayer thick. However, to have no energy barrier for the nucleation a very small and even zero contact angle would be ideal. When for example α- Al grows on a planar nucleant, the solid-liquid interface would form as a spherical cap and then the contact angle increases with the growth, it will reach a maximum and then it will only continue to grow if the curvature is reduced (Eqs. 5 and 6).
With the free growth theory the growth into a grain will occur if the maximum curvature is equal to 2/r* (where r* is the critical nucleus radius) and that is possible by increasing undercooling ΔT, which results in decreasing r*. If Eq. 21 is re-written where R_{nuc} is the radius of the planar circular face of the nucleant, then ΔT_{fg} would be the undercooling of free growth, which reflects the onset of free growth. Based on this equation (Eq. 36), the grain nucleates first on the largest nucleants [49].

$$\Delta T_{fg} = -\frac{2\sigma}{\Delta s R_{nuc}} \qquad \text{Eq. 36}$$

As described earlier, there are two different heterogeneous classic nucleation models proposed for the nucleation kinetics in metallic alloys; one for surface-dependent nucleation, the other for volume-dependent nucleation. Our cooling conditions gave ΔT_P = 7.1-18.7 K and $\dot{T} = 1.66 - 3.3\ K/s$, hence, it was assumed that the surface-dependent model was more applicable to our conditions. In addition to the use of classic nucleation to model the size of primary silicon particle, for the first time for this binary system, an alternative model concerning the inoculation in metallic system developed by Greer, namely free growth model [19] was employed. The modelling was validated using the post-solidification measurements of the number density for different casting and solidification conditions. It was found the free growth model gave a very good estimate whereas the Perepezko's model needed an assumed value for theta.

Moreover, assuming spherical-cap model, the contact angle changes only by the interfacial energy; however, the data applied to Perepezko's model showed it changes sensitively by undercooling. Any possible relation between the contact angle and undercooling was investigated using the published data for T_L, T_n, $\dot{T}$ and N_V from Liang et al [23], Kaneko et al [36], Ohmi et al [37-39], and the results of the present work in Perepezko's surface-dependent nucleation model (Eq. 9). Figure 8 plots the contact angle versus undercooling, showing theta is not constant at different undercoolings. Therefore, it is suggested that the Perepezko's nucleation model is not applicable for analyzing data in inoculated hypereutectic Al-Si alloy.

On the Perepezko model, each nucleant has a characteristic theta value; therefore, any change in theta (contact) angle with undercooling reflects that different inoculants are coming into operation. However, the results presented in Table 4 and Figure 10 show that the Perepezko model does not apply to them. There is a significant inconsistency between the predicted values with the measured data. For very small undercooling the predicted values are much smaller and for the high undercooling they are larger than the measured values.

In Contrast, the Greer's model predicts that only the largest nucleant particles will be effective as inoculants. By implication, the measured N_A selects just those particles - the ones that have been effective in nucleating primary silicon. Nevertheless, Greer’s model requires knowledge of the inoculant particles size and would be applicable more to conventional inoculation. It is believed [49] that it may fail if applied to rapid solidification or additive manufacturing where the nucleation mechanism and nucleants are less understood and are unclear.

Conclusions:

This work investigated nucleation behavior of primary silicon in a hypereutectic Al-Si alloy inoculated with AlP. It looked at the applicability of classic spherical model developed by Perepezko. For the first time, it used Free Growth model developed by Greer to predict the size of primary silicon particles, estimated data were compared with measured data obtained from optical micrographs. The results showed the following:

1. During solidification, the formation temperature is the most crucial variable in the Perepezko’s nucleation model applied to the nucleation of primary silicon in hypereutectic Al-Si alloys.
2. Assuming spherical-cap model, the contact angle changes only by the interfacial energy. However, the data applied to Perepezko’s model showed it changes by undercooling. Therefore, it is suggested that the Perepezko’s nucleation model might have not considered some parameters into account and hence it is not applicable for analyzing data in inoculated hypereutectic Al-Si alloy.
3. Greer’s free growth model was applied to model formation of primary silicon in hypereutectic Al-Si alloys and to predict their size. The results of this free growth model showed a reasonable approximation. Therefore, it is fair to say that for the studied condition, slow to intermediate cooling rate of hypereutectic Al-Si inoculated with P, Greer’s model should be used over classical nucleation model, but to be able to apply this model, the size of initial nucleants should be known.

Acknowledgement

MF is grateful for guidance and fruitful discussions with Emeritus Professor Howard Jones and Professor Iain Todd from the University of Sheffield during her PhD which encouraged her to investigate and take a new approach in numerical modelling of aluminum-silicon alloys treated by phosphorus, opposed to an earlier established model which seemed inadequate for this binary system.

References

1. J. Jorstad, and D. Apelian: *Int. J. Met.*, 2009, vol. 3 (3), pp. 13-36.
2. N. Tenekedjiev, and J.E. Gruzleski: *Cast Metals*, 1990, **3** (2), pp. 96-105.
3. F.L. Arnold, and J.S. Prestley: *AFS Trans.* 1961, vol. **69**, pp. 129-137.
4. Y. Telang: AFS Trans. 1963, vol. 71, pp. 232-240.
5. G.K. Sigworth: *AFS Trans.*, 1987, vol. **95**, pp. 303-314.
6. J.C. Weiss, and C.R. Loper Jr.: *AFS Trans.,* 1987, vol. **95**, pp. 51-62.
7. C.R. Ho, and B. Cantor: *Acta Metall. Mater., 1995, vol.* **43**, pp. 3231-3246.
8. K. Nogita, S.D. McDonald, K. Tsujimoto, K. Yasuda, and A.K. Dahle: *J. Electron Microscopy,* 2004, **53** (4), pp. 361-369.
9. K. Wang, X. Lü, Y.M. Zhu, H.Y. Jiang, Q.D. Wang, B. Ye, W.J. Ding: *Mater. Charact.*, 2019, 157 pp. 1-13.
10. Y. Xu, Y. Deng, D. Casari, R. H. Mathiesen, X. Liu, and Y. Li: *J. Alloys Compd.*, 2021, 854, P. 155323, 2021
11. W. Kasprzak, M. Sahoo, J. Sokolowski, H. Yamagata, and H. Kurita: *Int. J. Met.*, 2009, 3 (3), pp. 55-71.
12. W. Kasprzak, D. Sediako, M. Walker, M. Sahoo, and I. Swainson: *Metall. Mater. Trans. A*, 2011, 2 (7), pp. 1854-1862.
13. D. G. Sediako and W. Kasprzak: *Metall. Mater. Trans. A*, 2015, 46 (9), pp. 4160-4173.
14. M. W. Ullah and T. Carlberg: *J. Cryst. Growth*, 2011, 318 (1), pp. 212-218.
15. M. Faraji, I. Todd, and H. Jones: Met. Mat. Trans. A, 2009, vol. 40 (7), pp. 1710-1715.
16. D. Turnbull: *J. Chem. Phys.*, 1952, **20** (3) 1952, pp. 411-429.
17. J.H. Perepezko: in Metals Handbook, 9th edn, 1988, Vol. **15**, P. 101, ASM Metals Park, Ohio.
18. I. Maxwell, and A. Hellawell: *Acta Metall.* 1975, **23**, pp. 229-237.
19. A.L. Greer, A.M. Bunn, A. Tronche, P.V. Evans, and D.J. Bristov, *Acta Mater.*, 2000, **48**, pp. 2823-2835.
20. W.J. Kyffin, W.M. Rainforth, and H. Jones: Mat. Sci. Tech., 2001, 17 (8), pp. 901-905.
21. J.W. Martin, "Micromechanisms in particle-hardened alloys", Cambridge University Press, Cambridge, UK, 1980, p. 142.
22. J.L. Murray, and A.J. McAlister, *Bull. Alloy Phase Diagrams,* 1984, **5**, pp. 74-84.
23. D. Liang, Y. Bayraktar, and H. Jones: *Acta Metall. Mater.*, 1995, 43 (2), pp. 579-585.
24. D. Turnbull: *J. Chem. Phys.*, 1950, 18, 2, pp. 198-203.
25. D. Turnbull, and B. Vonnegut: Industr. Eng. Chem., 1952, vol. 44 (6), pp. 1292-1298.
26. D. Turnbull: *J. App. Phys.*, 1950, 21, pp. 1022-1028.
27. J.H. Perepezko, and W.S. Tong: *Phil. Trans. R. Soc. Lond.*, 2003, A 361, pp. 447-461
28. M. Gremaud, D.R. Allen, M. Rappaz, and J.H. Perepezko: *Acta Mater.*, 1996, **44** (7), pp. 2669-2681.
29. H. Vekhamäki, A. Määttänen, A. Lauri, I. Napari, and M. Kulmala: *Atmos. Chem. Phys. Discuss.*, 2006, **6**, pp. 9069–9083.
30. D. Turnbull: 1953, *Acta Metall.*, **1** (1), pp. 8-14.

31. W.J. Boettinger, and J.H. Perepezko: 1985, in Rapidly Solidified Crystalline Alloys, ed. by S.K. Das, B.H. Kear, C.M. Adam, TMS, Warrendale, PA, p.24.
32. J.H. Perepezko, and G. Wilde: *Curr. Opin. Solid State Mater. Sci.,* 2016, 20, pp. 3-12.
33. J.P. Hirth: *Met. Trans. A*, 1978, **9**, pp. 401-404.
34. C.R. Ho, and B. Cantor: *Mater. Sci. Eng* A, 1993, **173**, pp. 37-40.
35. M. Faraji, I. Todd, and H. Jones: *J. Mater. Sci.*, 2005, **40**, (24), pp. 6363-6365.
36. J. Kaneko, M. Sugamata, and K. Aoki: *Trans. Jpn. Inst. Met.* 1979, **20**, pp. 734-741.
37. T. Ohmi, Y. Tanaka, M. Kudoh: *Bull. Fac. Eng. Hokkaido Univ.*, 1991, **156**, pp. 1-10.
38. T. Ohmi, M. Kudoh, K. Ohsasa, Y. Itoh, K. Matsuura, and K. Ishii: *J. Jap. Inst. Light Metals*, 1994, **44**, (2), pp. 91-96.
39. T. Ohmi, K. Matsuura, M. Kudoh, and Y. Itoh: *Jap. Inst. Light Metals*, 1997, **47**, (2), pp. 71-77.
40. C.V. Thompson, and F. Spaepen: *Acta Metall.,* 1983, **31**, pp. 2021-2027.
41. X. Yao, A.K. Dahle, C.J. Davidson, and D.H. StJohn, *J. Mater. Res.*, 2006, **21** (10), pp. 2470-2479.
42. A.L. Greer, T.E. Quested, and J.E. Spalding, in Light Metals 2002 as held at the 2002 TMS Annual Meeting ed. by W.A. Schneider (TMS, Warrendale, PA), 2002, pp. 687-694.
43. M. Gündüz and J.D. Hunt: *Acta Metall.*, 1985, **33** (9), pp. 1651-1672.
44. S.A. Moir and H. Jones: *J. Cryst. Growth*, 1991, 113 (1-2), pp. 77-82.
45. W.J. Kyffin, W.M. Rainforth, and H. Jones: *Z. Metallkd.*, 2001, **92** (4), pp. 396-398.
46. O. Kubaschewski and C.B. Alcock: Metallurgical Thermochemistry, International Series of Materials Science and Technology, Vol 24, Fifth Edition, Edited by G.V. Raynor, Pergamon Press Ltd, 1979, UK, pp. 336-339.
47. S.-I. Fujikawa, K.-I. Hirano, and Y. Fukushima: *Metall. Trans. A.*, 1978, vol. 9, pp. 1811-1815.
48. A.L. Greer: in Solidification of Aluminum Alloys as held at the 2004 TMS Annual Meeting; Charlotte, NC; USA; 14-18 Mar. 2004, ed. by M.G. Chu, D.A. Granger and Q. Han, pp. 131-146.
49. A.L. Greer: *J. Chem. Phys.*, 2016, 145 (21), p. 211704.
50. P.V. Evans, and S.R. Stiffler: *Acta Metall. Mater.*, 1991, 39 (11), pp. 2727-2731.
51. C.J. Smithells: Smithells Metals Reference Book, 1983, London, Butterworths.
52. M. Petrescu: *Z. Metallk.*, 1970, 61, pp. 14-18.

Table 1 The quantitative results obtained from cooling curves and quantitative metallography for the studied conditions. Different coding used for samples cast in different molds are as follows: C, D and S represent samples cast in sand molds, alumina molds and steel molds, respectively.

No	Sample	Mold	Addition	Process	T_n (°C)	$\dot{T}$ (K/s)	ΔT (K) $=T_L- T_n$	N_A (/mm^2)	N_V (/mm^3)
1	C1	Sand	…..	Bottom casting	654.8	2.92	5.9	28±15	226±180
2	C2	Sand	…..		654.0	2.02	6.7	27±18	214±210
3	C3	Sand	…..		652.5	2.50	8.2	36±28	330±374
4	C4	Sand	…..		653.3	2.42	7.4	30±22	251±269
Average:					**653.6±1.1**	**2.46±0.37**	**7.1±1.0**	**30±4**	**255±52**
5	C5	Sand	0.02 wt% P		648.6	2.70	12.1	31±28	264±342
6	C6	Sand	0.02 wt% P		651.7	2.10	9.0	39±20	372±283
7	C7	Sand	0.02 wt% P		654.2	2.87	6.5	48±31	508±483
8	C8	Sand	0.02 wt% P		652.0	2.81	8.7	40±19	387±273
Average:					**651.6±2.3**	**2.62±0.35**	**9.1±2.3**	**40±7**	**383±100**
16	D1	Alumina	…..	Chamber furnace				42±24	416±351
17	D3	Alumina	…..		653.9	1.59	6.8	31±19	264±238
18	D5	Alumina	…..		647.1	1.71	13.6	32±17	277±218
Average:					**650.5±4.8**	**1.65±0.08**	**10.2±4.8**	**35±6**	**319±84**
19	D2	Alumina	0.02 wt% P					65±28	801±513
20	D4	Alumina	0.02 wt% P		659.8	1.73	0.9	54±19	607±318
					659.8	**1.73**	**0.9**	**60±8**	**704±137**
21	S1	Steel	…..	Chamber furnace	646.0	1.98	14.7	29±17	239±207
22	S2	Steel	…..		654.5	2.24	6.2	36±18	330±245
23	S3	Steel	…..		655.0	2.08	5.7	26±17	203±195
Average:					**651.8±5.1**	**2.10±0.13**	**8.9±5.1**	**30±5**	**257±65**
24	S4	Steel	0.02 wt% P		642.3	2.60	18.4	35±20	316±267
25	S5	Steel	0.02 wt% P		632.0	1.95	28.7	49±20	524±319
26	S6	Steel	0.02 wt% P		638.3	2.63	22.4	41±23	401±333
27	S13	Steel	0.02 wt% P		655.3	2.20	5.4	45±17	461±260
28	S14	Steel	0.02 wt% P		632.0	2.39	28.7	35±15	316±202
29	S15	Steel	0.02 wt% P		652.5	1.97	8.2	40±24	387±342
Average:					**642.1±10.1**	**2.29±0.30**	**18.6±10.0**	**40±6**	**400±82**
30	S7	Steel	0.04 wt% P		650.8	2.57	9.9	56±21	641±358
31	S8	Steel	0.04 wt% P		652.1	2.46	8.6	55±20	623±338
32	S9	Steel	0.04 wt% P		652.9	2.60	7.8	61±12	728±215
Average:					**651.9±1.1**	**2.54±0.07**	**8.8±1.1**	**57±3**	**664±56**
33	S10	Steel	0.08wt% P		652.1	2.17	8.6	65±24	801±441
34	S11	Steel	0.08wt% P		650.1	2.28	10.6	61±14	728±250
35	S12	Steel	0.08wt% P		651.4	3.26	9.3	51±10	557±163
Average:					**651.4±1.0**	**2.57±0.60**	**9.5±1.0**	**59±7**	**694±125**

T_n: formation temperature of Primary Si, Tdot: cooling rate from peak temp. to T_n, ΔT Undercooling for Primary Si,

Table 2 Al-Si thermodynamic model parameters, J/mol, T in K (data is taken from Ref. 22).

${}^{0}G_{Al}^{fcc} = -10792$	$A^{L} = -10695.4$
${}^{0}G_{Si}^{fcc} = 12.12T$	$B^{L} = -4275.5 + 3.044T$
${}^{0}G_{Si}^{dia} = -50600$	$C^{L} = 670.7 - 0.460T$
${}^{0}G_{Al}^{dia} = 30.00T$	$A^{fcc} = -200 - 7.594T$
${}^{0}G_{Al}^{L} = 0$	$A^{dia} = 89138$
${}^{0}G_{Si}^{L} = 0$	

Table 3 Required data used in Perepezko nucleation model for the nucleation of primary silicon in solidification of hypereutectic Al-Si.

Parameter	**Symbol**	**Value**	**Reference**
The Surface-Dependent Model			
S/L interfacial energy	σ_{SL}	0.344 J/m^2	[50]
Atomic jump distance for attachment of Si from the melt	a	3×10^{-10} m	[51]
Activation enthalpy for diffusion of Si in liquid Al-Si	Q	25740 J/mol	[52]
Diffusivity in the melt	D_L	2.08×10^{-7} exp (-25740/8.314T) m^2/s	[51]
Number of surface atoms of the nucleation site per unit volume of melt	ρ (in other sources N_0)	10^{20} m^{-3}	[23]
The Volume-Dependent Model (Using Gremaud et al [28])			
S/L interfacial energy	σ_{SL}	0.3524 J/m^2	[43]
Base levels of nucleants	N_v^0	10^{13} m^{-3}	[28]
Nucleant potency parameter	B	0.0590 K^{-1}	[28]
Nucleant particle area	A_P	3.14×10^{-16} m^2	[28]
Zeldovich factor	Z	0.0198	[28]

Table 4: The results of size predictions for 15 different casting conditions using Perepezko's surface dependent nucleation model; The values for theta are gathered using equation 17.

Sample	**ΔT (k)**	**Predicted theta (°)**	**r_M: Measured radius (μm)**	**r_P: Predicted radius (μm)**	**Ratio: r_M/r_P**
S1	14.7	28.32	49.7	33.5	1.81
S2	6.2	22.65	44.5	0.6	88.55
S3	5.7	22.23	52.4	0.2	281.10
S4	18.4	27.64	45.2	105.7	0.52
S5	28.7	30.38	38.2		
S6	22.4	32.38	41.7		
S13	5.4	22.03	39.8	0.2	242.57
S14	28.7	31.16	45.2	216.4	0.27
S15	8.2	24.12	42.2	1.1	48.22
S7	9.9	25.30	35.7		
S8	8.6	24.40	36.0		
S9	7.8	23.83	34.2		
S10	8.6	24.40	33.1	1.4	29.98
S11	10.6	25.77	34.2	3.7	11.19
S12	9.3	24.89	37.4	4.0	11.42

Table 5: Thermodynamic parameters used in present calculations for Al-Si alloys [46, 51], values were given in cal/mol K, they were converted to J/mol K to be used in the calculations

Property S^0_{298}	**Value (unit)**	**Property S^0_{298}**	**Value (unit)**
<Si> (solid)	18.84 J/mol K	**<Al> (solid)**	28.33 J/mol K
(Si) (Liquid)	168.5 J/mol K	**(Al) (Liquid)**	165.06 J/mol K
$C_P = a + bT + cT^{-2}$ (J/molK)			
	A	**b× 10^3**	**c × 10^{-5}**
Al (solid)	20.67	12.39	
Al (liquid)	31.80		
Si (solid)	23.93	2.47	-4.14
Si (liquid)	25.61		

Table 6: The results of size predictions for 15 different casting conditions using Greer's nucleation model.

Sample	**ΔT (k)**	**r_M: Measured radius (μm)**	**r_P: Predicted radius (μm)**	**Ratio: r_M/r_P**
S1	14.7	49.7	39.2	1.27
S2	6.2	44.5	36.3	1.23
S3	5.7	52.4	40.2	1.30
S4	18.4	45.2	34.4	1.31
S5	28.7	38.2	37.5	1.02
S6	22.4	41.7	34.1	1.22
S13	5.4	39.8	40.0	0.99
S14	28.7	45.2	36.1	1.25
S15	8.2	42.2	38.0	1.11
S7	9.9	35.7	35.7	1.00
S8	8.6	36.0	36.5	0.99
S9	7.8	34.2	36.0	0.95
S10	8.6	33.1	39.3	0.84
S11	10.6	34.2	37.4	0.91
S12	9.3	37.4	34.6	1.08